Materials Letters 114 (2014) 44–47

Contents lists available at ScienceDirect

Materials Letters

journal homepage: www.elsevier.com/locate/matlet

Room temperature ferromagnetism in Mn-doped TiO_2 nanopillar matrices

Meredith C.K. Sellers, Edmund G. Seebauer *

Department of Chemical & Biomolecular Engineering, University of Illinois at Urbana-Champaign, 600 S. Mathews Ave., Urbana, IL 61801, USA

ARTICLE INFO

Article history:
Received 31 July 2013
Accepted 26 September 2013
Available online 5 October 2013

Keywords:
Ferromagnetism
TiO_2
Grain boundaries
Nanocrystalline materials
Semiconductors

ABSTRACT

Diluted magnetic semiconductors have attracted considerable attention for potential applications in spintronics. Morphology and microstructure exert strong, but complicated, effects upon ferromagnetic behavior. To partially unravel such effects, the present work compares room temperature ferromagnetism (RTFM) in Mn-doped anatase TiO_2 films synthesized by two different atomic layer deposition protocols, leading to either nanopillars or more conventional columnar grains. RTFM is largely unaffected by this difference for undoped material, but nanopillaring greatly increases both the coercive field (100 Oe) and saturation magnetization (14–21 emu/cm^3) for Mn doping up to 2.7 at%. Nanopillaring seems to enhance the congregation of defect-related bound magnetic polarons near grain boundaries, thereby increasing RTFM.

1. Introduction

Diluted magnetic semiconductors (DMSs) have attracted considerable attention as promising materials for spintronics-based data storage and logic devices [1]. Morphology [2] and microstructure [3] exert strong effects upon ferromagnetic behavior in DMSs in ways that could be exploitable. However, the effects are complicated. In DMSs such as TiO_2, ZnO, and CeO_2 doped with open-shell transition metal elements, ferromagnetism depends not only upon the dopant, but also upon native point defects [4] and extended defects [5,6]. For example, F^+ centers (electrons in singly occupied oxygen vacancies, V_O) and Ti^{3+}–V_O complexes help mediate ferromagnetism in anatase TiO_2 powders [7]. The concentrations and electrical activities of dopants and point defects depend strongly on synthesis protocols [8], so the distinctive contributions of each factor are not easily unraveled. Grain boundaries further complicate the mix, and yet these extended defects play especially important roles in DMSs that have special nanostructuring such as nanopillars or nanorods. The present work seeks to unravel some of these effects in the case of Mn-doped anatase TiO_2.

Mn-doped TiO_2 exhibits especially complex effects of microstructure and atomic ordering on room temperature ferromagnetism (RTFM). For example, RTFM disappears when the growth rate of the anatase form by plasma-assisted molecular beam epitaxy decreases from 0.2 to 0.08 Å/s [9]. For such material (3.4–3.5 at% Mn), the decrease in growth rate leads to more uniform crystallographic orientation and the complete disappearance of the rutile polymorph. However, the rutile polymorph (2.5 at% Mn) exhibits stronger RTFM than pure anatase when prepared by the sol–gel method [10]. A similar increase has been observed for TiO_2 (B) versus anatase phase in hydrothermally-prepared polycrystalline Fe-doped TiO_2 nanorods [4]. Curiously, Mn-doped anatase formed by spray pyrolysis exhibits RTFM only above 5 at% Mn, and displays a non-monotonic variation in magnitude with Mn concentration [11].

The present work compares the RTFM behavior of polycrystalline TiO_2 films grown by atomic layer deposition (ALD) under two protocols: deposition at 400 °C (which yields nanopillared crystalline material) and deposition at 200 °C (which yields amorphous material) followed by annealing at 550 °C to induce crystallization. The RTFM of material prepared via the latter protocol has been described previously [12], so the present work details the behavior of the 400 °C material and highlights the comparisons and contrasts. We note that nanopillared oxides have shown special promise for spintronics applications [13,14].

2. Experimental

Undoped and Mn-doped TiO_2 were synthesized on commercial n-type Si(100) (Sb, 0.013 Ω cm resistivity, 2 cm × 2 cm) by ALD at 400 °C. The precursors were $Ti(OCH(CH_3)_2)_4$ (TTIP, Strem Chemicals Inc., 98%), H_2O (DI, no further purification), and $Mn(DPM)_3$ (DPM = 2,2,6,6-tetramethyl-3, 5-heptanedionato, Strem Chemicals Inc., 99%), with N_2 (SJ Smith, 99.999%) serving as the carrier gas [8].

* Corresponding author. Tel.: +1 217 244 9214; fax: +1 217 333 5052.
E-mail address: eseebaue@illinois.edu (E.G. Seebauer).

0167-577X/$ - see front matter © 2013 Elsevier B.V. All rights reserved.
http://dx.doi.org/10.1016/j.matlet.2013.09.097

$Mn(DPM)_3$ was evaporated from a porous filter enclosure within the vacuum chamber. The supply rate of the Mn source was controlled indirectly by changing the distance between the filter enclosure and the resistively heated substrate platform. A full ALD cycle consisted of a TTIP pulse (8 s), N_2 purge (10 s), H_2O pulse (8 s), and another N_2 purge (10 s).

Film thickness was measured by a Rudolph Technologies AutoEL III ellipsometer. Film morphology was investigated using a Hitachi S4800 scanning electron microscope (SEM). X-ray photoelectron spectroscopy (XPS) was performed with a Kratos AXIS Ultra (40 eV, Al Kα). Peak deconvolution and fitting was carried out with CasaXPS software; the binding energy (BE) scale was calibrated using the C *1s* line at 285.0 eV. X-ray diffraction (XRD) and X-ray reflectivity (XRR) patterns were obtained with a high-resolution Philips X'Pert diffractometer ($\lambda = 0.15406$ nm) (45 kV, 40 mA, Cu Kα1). For the analysis described here, it was assumed that peak broadening was due to crystallite size only (i.e., contributions from strain were neglected). Values of bulk density were obtained by XRR fitting [15]. Magnetization measurements were carried out at 27 °C using a SQUID magnetometer (Quantum Design Model MPMS-XL). The magnetic field was applied parallel to the film plane.

3. Results

Cross-sectional morphologies of typical 100 nm undoped and Mn-doped TiO_2 deposited on Si(100) at 400 °C are shown in Fig. 1 (a) and (b). The micrograph for undoped TiO_2 reveals high aspect ratio columns approximately 20 nm in width with discernible inter-column spacing in the lateral direction. Direct nanopillar evolution occurs without substrate masking or catalyst seeding, as has been noted for substantially thicker TiO_2 (1.2 μm) grown on sapphire (100) by chemical vapor deposition (CVD) [16]. In-situ Mn doping during TiO_2 deposition at 400 °C leads to slight degradation of the high aspect ratio pillars (Fig. 1(b)). The nanopillars still appear vaguely columnar, but increase in width to approximately 40 nm. The visible void fraction in the matrix decreases, and the high aspect ratio columns start to merge together laterally.

Fig. 1(c) shows Ti 2*p* XPS spectra for TiO_2 with 0.0–3.0 at% Mn. For undoped and minimally doped (< 2.0 at% Mn) TiO_2, the 5.7 eV-spaced Ti $2p_{3/2}$ and $2p_{1/2}$ peaks situated at 458.5 and 464.2 eV indicate the presence of Ti^{4+} ions. At higher doping levels (> 2.0 at% Mn), the Ti $2p_{3/2}$ and $2p_{1/2}$ peaks shift downward by ~0.5 eV. This shift, and concurrent peak broadening, has been noted [17] to arise following dopant incorporation into the lattice, which prompts Ti^{4+} ions to release electrons in order to reestablish charge equilibrium. XPS also indicates a change in oxygen stoichiometry with Mn doping; the ratio of lattice oxygen to titanium is 1.98, 2.05, and 2.35 for 0.0, 1.4, and 2.7 at% Mn-doped TiO_2. The XPS spectra in Fig. 1(d) reveal Mn $2p_{3/2}$ and $2p_{1/2}$ core-levels at 641.2–641.5 and 653.0–653.2 eV, respectively. In both cases, the satellite structure in the 647 eV range suggests the presence of divalent Mn ions; the Mn $2p_{3/2}$ binding energy values themselves indicate that Mn is also present as Mn^{3+}, consistent with other reports [18,19].

Fig. 2(a) shows XRD patterns for undoped and Mn-doped TiO_2. The nanopillar matrices are polycrystalline anatase with (101), (200), and (211) orientations (JCPDS Card no. 21-1272). Since diffraction peak positions are governed by the spacing between planes of atoms, the observed shift in peak position with doping suggests a change in interplanar spacing i.e., lattice parameter. Here, the incorporation of Mn into the TiO_2 crystal lattice manifests as a decrease in the unit cell volume from 136.8 to 133.9 $Å^3$ (for 2.7 at% Mn) (Fig. 2(b)). Considering the ionic radii of Ti^{4+} (0.61 Å) and Mn^{3+} (0.58 Å) [20] and Vegard's law, dopant atoms

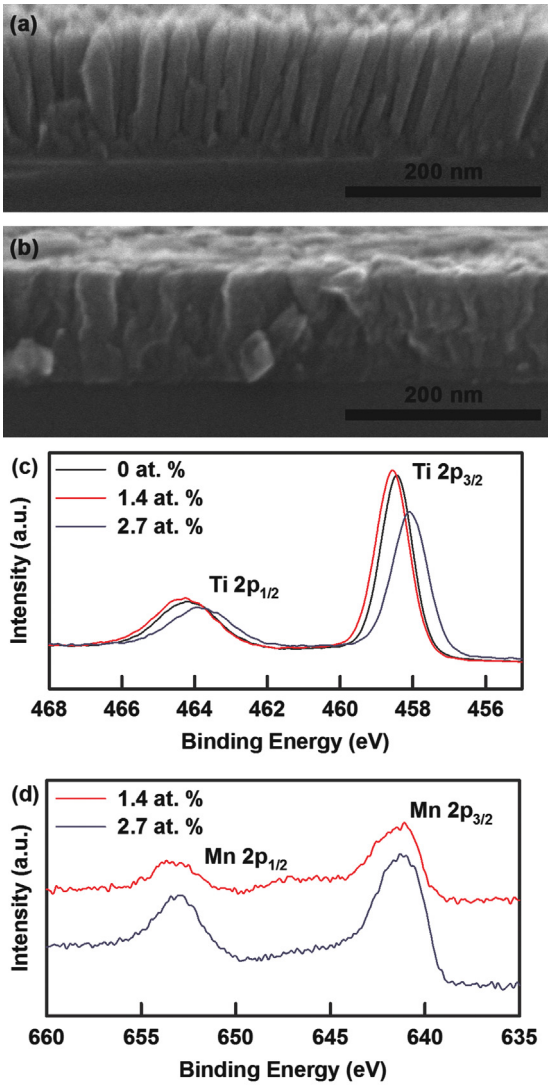

Fig. 1. Typical cross-sectional micrographs of ~100 nm thick (a) undoped and (b) Mn-doped TiO_2 as well as XPS spectra of (c) Ti 2*p* core-levels and (d) Mn 2*p* core-levels in undoped and Mn-doped TiO_2.

are likely incorporated at Ti^{4+} lattice sites. The comparatively smaller Mn^{3+} radius causes a contraction of the crystal lattice and concordant shift in the (101) diffraction peak. Despite changes in nanopillar morphology, the average crystallite size in the film growth direction remains fairly constant with Mn addition (Fig. 2(c)); values of 27.9 ± 1.5, 28.4 ± 1.7, and 26.4 ± 2.0 nm were obtained for 0.0, 1.4, and 2.7 at% Mn-doped TiO_2. The same thing cannot be said for bulk density; XRR spectral fitting reveals that undoped, 1.4, and 2.7 at% Mn-doped TiO_2 have densities of 2.8 ± 0.14, 3.34 ± 0.17, and 3.95 ± 0.20 g/cm^3, respectively (Fig. 2(d)). For comparison, the bulk density of single crystal anatase is 3.89 g/cm^3.

Fig. 3(a) shows magnetization–magnetic field (*M*–*H*) data acquired at room temperature for both doped and undoped anatase. The undoped material exhibits a weak ferromagnetic characteristic, with coercive field (H_c) and saturation magnetization (M_s) values of 50 Oe and 3.8 emu/cm^3, respectively. Doping causes H_c to grow substantially to ~100 Oe. Similarly, M_s increases by almost an order of magnitude to 21 and 14 emu/cm^3 for 1.4 and 2.7 at% Mn doping, in that order. Remnant magnetization (M_r) values were similarly elevated upon Mn doping: 0.10, 5.5, and 3.4 emu/cm^3 for 0.0, 1.4, and 2.7 at% Mn-doped TiO_2.